# THE HRSC DTM TEST

C. Heipke[1*], J. Oberst[2], J. Albertz[5], M. Attwenger[3], P. Dorninger[3], E. Dorrer[4], M. Ewe[2], S. Gehrke[5], K. Gwinner[2], H. Hirschmüller[6], J.R. Kim[7], R.L. Kirk[8], H. Mayer[4], J.-P. Muller[7], R. Rengarajan[9], M. Rentsch[4], R. Schmidt[1], F. Scholten[2], J. Shan[9], M. Spiegel[10], M. Wählisch[2], G. Neukum[11] and the HRSC Co-Investigator Team.

[1] Institute of Photogrammetry and GeoInformation (IPI), Leibniz Universität Hannover
[2] German Aerospace Center (DLR), Institute of Planetary Research, Berlin
[3] Institute of Photogrammetry and Remote Sensing (ipf), Vienna University of Technology
[4] Institute for Photogrammetry and Cartography, Munich Bundeswehr University
[5] Institute for Geodesy and Geoinformation Science, Technische Universität Berlin
[6] German Aerospace Center (DLR), Institute of Robotics and Mechatronic, Oberpfaffenhofen
[7] Department of Geomatic Engineering, University College London (UCL)
[8] Astrogeology Team, United States Geological Survey (USGS), Flagstaff
[9] Geomatics Engineering, Purdue University
[10] Photogrammetry and Remote Sensing, Technical University Munich
[11] Institute of Geological Sciences/Planetology, Freie Universität Berlin

**Working Group IV / 7**

**KEY WORDS**: HRSC, Mars, surface reconstruction, DTM/DEM, experimental test

**ABSTRACT:**
The High Resolution Stereo Camera (HRSC) has been orbiting the planet Mars since January 2004 onboard the ESA Mars Express mission and delivers imagery which is being used for topographic mapping of the planet. The HRSC team is currently conducting a systematic inter-comparison of different alternatives for the production of high resolution Digital Terrain Models (DTMs) from the multilook HRSC push broom imagery. Based on carefully chosen test sites the test participants have produced DTMs which have been subsequently analysed in a quantitative and a qualitative manner. This paper reports on the results obtained in this test.

## 1. INTRODUCTION

The *High Resolution Stereo Camera* (HRSC, Neukum et al., 2004) is part of the orbiter payload on the *Mars Express* (MEX) mission of the European Space Agency (ESA), orbiting the Red Planet in a highly elliptical orbit since January 2004. For the first time in planetary exploration, a camera system has especially been designed to meet the requirements of photogrammetry and cartography for mapping the complete surface of a planet (Albertz et al., 2005). For this purpose HRSC operates as a push broom scanning instrument with 9 CCD line detectors mounted in parallel in the focal plane of the camera. Data acquisition is achieved by five panchromatic channels under different observation angles and four colour channels. At periapsis the ground resolution of the nadir channel amounts to 12.5 m, the stereo channels are typically operated at a 2x coarser resolution with the two photometry and the four colour channels at 4x or 8x coarser resolution. The data provided by HRSC are well suited for the automatic generation of *Digital Terrain Models* (DTMs) and other 3D data products. Such products are of vital interest to planetary sciences. As the Mars Express mission has recently been extended to a lifetime of four years the prospects for a complete topographic mapping of Mars by HRSC at very high resolution are currently very good, indeed.

Image matching is well researched and has been documented in the literature. In general, it is agreed that in “simple” terrain (sufficient grey value variation, not too rough terrain) and with adequate image acquisition geometry (similar flying height, similar direction of optical axes, known relative image rotation if any), very good results can be achieved by totally automated approaches: the matching completeness in these areas reaches 100 %, at a density of various pixels per DTM grid mesh, and the geometric accuracy is well below one pixel. Things start to be much more complicated if more complex situations are faced, such as steep terrain, height discontinuities, occlusions, poor texture, shadows, atmospheric dust, clouds, increased image noise, compression artefacts etc., some of which are commonplace in HRSC images.

Nevertheless, automatic DTM generation from HRSC images by means of image matching has reached a very high level over the years. The systematic processing chain at DLR for producing preliminary DTMs with 200 m resolution (Scholten et al., 2005) runs well and stable. In addition, several groups are able to produce DTMs using different approaches, or have developed alternative modules for parts of the DTM generation process (Albertz et al., 2005). Also, some of these groups are developing shape from shading techniques, of which one example was available in time to be included here.

In some cases, these approaches are still experimental and so currently limited to small areas. It is against this background that the desire was expressed to compare the individual approaches for deriving DTMs from HRSC images in order to assess their advantages and disadvantages.

## 2. TEST GOALS AND ORGANISATION

For generating a DTM a number of different steps must be carried out. The principal ones are

- image pre-processing (an optional step comprising radiometric noise reduction and pre-rectification),
- image matching,
- generation of a 3D point cloud, and
- DTM interpolation onto a regular grid.

While it is interesting to study these steps in detail it was decided that this test would take a more general view and

* Corresponding author, heipke@ipi.uni-hannover.de

analyse only the resulting DTMs. The reason is that several of the approaches do not yield comparable intermediate products, and thus a detailed study was not deemed feasible. In addition, reports examining the individual steps of DTM generation can be found in the literature, albeit not necessarily for planetary images.

Key goals of the test were the reconstruction of fine details and the geometric accuracy of the DTMs. Fine detail is studied using a variety of qualitative assessments in small but representative areas, while geometric accuracy is analysed with respect to the MOLA DTM (Mars Orbiter Laser Altimeter, Zuber et al., 1992; Smith et al., 2001). This DTM is the most consistent Mars DTM available to date. Note that the geometric analysis suffers from the lack of a reference data set with superior accuracy, mainly because the MOLA DTM does not have an adequate planimetric resolution. The quantitative results presented in this paper therefore relate to the differences between the HRSC DTM and MOLA DTM, and incorporate the inaccuracies inherent in both sources. In addition, many groups used MOLA information already as input for their procedures[1], making an independent check of the results somewhat questionable. Nevertheless, such computations are useful, because differences in the results from participant to participant can be linked to the individually generated HRSC DTMs. All quality parameters were also related to operational aspects such as the computing effort of the applied method, and thus its applicability to generating DTMs of large areas (multiple orbits, potentially the whole HRSC data set).

The test was organised by the Photogrammetry and Cartography Working Group within the HRSC Co-Investigator team under the auspices of the ISPRS Working Group IV/7 on *Extraterrestrial Mapping.* IPI, University of Hannover, and DLR Berlin-Adlershof acted as pilot centres for the test. Based on commonly agreed test data sets including image orientations refined by bundle adjustment, a total of seven groups have derived DTMs. The pilot centres then analysed the data produced. To our knowledge this is the first multi-site test for DTM generation from planetary imagery.

## 3. TEST DATA

Two data sets were chosen for the test. These are the HRSC images h1235_0001[2], and a block of three adjacent images, numbered h0894_0000, h0905_0000, and h0927_0000[2] (see also Table 1). In addition to the processing of complete orbit images, sub-areas were defined for contributions of limited areas (Figure 1). The sub-area in image 1235 covers western Candor Chasma at approximately -8° to -4°N and 282° to 284°E, and includes the spectrally distinctive Ceti Mensa. This sub-area exhibits many steep slopes and a number of horizontal plateaus with very little texture (see Figure 1, left). The second sub-area covers Nanedi Vallis at approximately 2.5° to 7.5°N and 310° to 314°E. In this area many craters of different size are visible (see Figure 1, right). In addition to being scientifically interesting the Nanedi orbits provide a test of capabilities for producing seamless DTMs from blocks of images.

In general, the image quality of the Nanedi orbits is good, whereas the Candor Chasma image exhibits lower contrast and some image noise. While most image data were free of errors, all channels of image 927 contained gaps (areas for which no grey values had been recorded), most of them having a duration of less than 2 s (equivalent to 488 image lines). In addition, the backward stereo channel (stereo 2) contained a gap of 45 s corresponding to over 6000 image lines. Furthermore, the integration time was changed during image acquisition[3]. Among other reasons this image was chosen in order to investigate how the individual matching approaches would cope with such challenges.

In addition to the images, orientation parameters were provided to the participants. The HRSC sensor model developed at DLR was used to describe the interior orientation. Exterior orientation parameters were derived from a bundle adjustment (Schmidt et al., 2005; 2006; Spiegel et al., 2005; 2006). Since the bundle adjustment uses MOLA data as control information, the resulting orientation parameters automatically tie the surface derived from image matching to the MOLA DTM. The theoretical standard deviation of the bundle adjustment for the complete orbits was about 25 m in planimetry (Candor and Nanedi) and 50 m (Candor) respectively 30 m (Nanedi) in height. The participants were encouraged to use these orientation parameters, but were free to determine their own interior and exterior image orientation.

All DTMs delivered back to the pilot centre were to be derived in the sinusoidal map projection using the MOLA sphere (radius: 3396 km) as the lateral and vertical reference surface.

## 4. TEST PARTICIPANTS AND APPROACHES USED FOR GENERATING DTMS

Altogether seven groups agreed to participate in the test (see Table 2). Some of them delivered two sets of results, some processed the complete orbits, and others restricted their efforts to single orbits or sub-areas. The individual approaches are described in existing literature. Due to lack of space, only a short summary is provided here.

**DLR-Scholten** (Scholten et al., 2005): *Image pre-processing* consists of an optional box filtering (carried out in V.1, but not in V.2) and a pre-rectification of the images using the MOLA DTM. Least-squares *image matching* is done pair-wise between the nadir channel and the four additional panchromatic channels (stereo and photometry). Point tuples are subsequently generated and *3D points* are computed by least squares forward intersection. A threshold for the intersection accuracy is applied to eliminate blunders. After *interpolating the DTM,* box filtering was employed to reduce artefacts (only in version 1).

[1] MOLA is used as control information in the bundle adjustment, as a surface for pre-rectification prior to matching, for fitting results of individual strip DTMs and for filling holes resulting from matching blunders. The degree to which the participants made use of MOLA varies (see section 4).

[2] The notation refers to the file name convention used in the HRSC experiment. Image h1235_0001 was acquired in orbit 1235. In this orbit the HRSC was switched on twice resulting in images h1235_0000 and h1235_0001. The latter one was used in this study. The names of the Nanedi images follow the same convention. In the remainder of the paper only the orbit numbers are used to identify the images, since no ambiguity can arise. In all cases the so called "bested" version (i.e. the archival quality version) was provided to the participants.

[3] Changing integration times are used rather frequently in the HRSC experiment (not for 1235, however). Due to the highly elliptical Mars Express orbit the ground resolution changes as a function of time. Whereas the across track pixel dimension on the ground cannot be influenced, the along track dimension is a function of the integration time. Changes in integration time thus allow for acquiring square pixels.

| | | Candor Chasma | Nanedi Vallis |
|---|---|---|---|
| HRSC orbit | | 1235 | 894; 905; 927 |
| ground resolution | nadir | 21–32 m | 14–23 m |
| | stereo (2) | 42–80 m | 28–55 m |
| | photometry (2) | 84–146 m | 55–102 m |
| | colour (R, G, B, NIR) | 168–306 m | 54–106 m |
| no. of lines of complete image (nadir) | | 74 144 | 45 272; 51 136; 57 856 |
| area covered by complete image | | 1987 × 139 $km^2$ | 885 × 101; 936 × 95; 976 × 87 $km^2$ (indiv. images)<br>880 × 260 $km^2$ (mosaic) |
| no. of lines of sub-area (nadir) | | 11 000 | 12 300 |
| area covered by sub-area | | 275 × 150 $km^2$ | 300 × 93; 300 × 90; 300 × 82 $km^2$ (indiv. images)<br>300 × 240 $km^2$ (mosaic) |

Table 1: Description of the test data

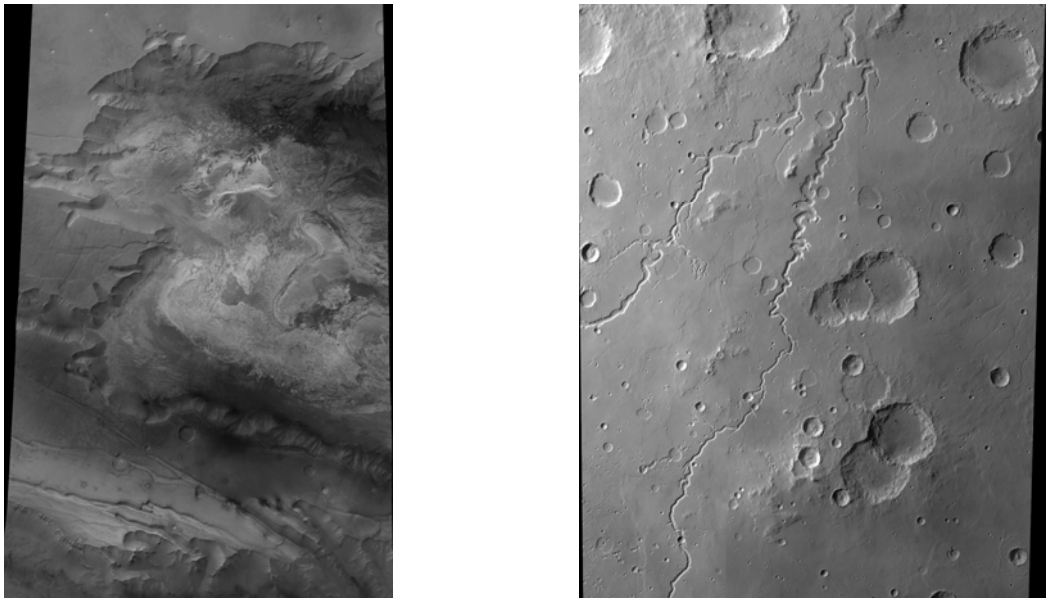

Figure 1: Orthophotos of the sub-areas derived from the nadir channel: Candor Chasma (left, image h1235_0001), Nanedi Vallis (right, images h927_0000, h905_0000 and h894_0000 from left to right). Both images are oriented towards North.

| **Participant** | | **Processed area** | **Used software** |
|---|---|---|---|
| DLR-Scholten | V.1: standard | complete orbits | DLR approach for preliminary DTMs, except for refined ext. ori. par. and fit of strips to MOLA |
| | V.2: no noise reduction in images, no post-filtering | | |
| DLR-Gwinner | V.1: removal of blunders detected by ipf | complete orbits | refined DLR approach |
| | V.2: no blunder detection by ipf | | |
| DLR- Gwinner / ipf | 3D points from DLR-Gwinner as input | complete orbits | self developed blunder detection + SCOP |
| DLR-Hirschmüller | | complete orbits | self developed |
| Purdue | | complete orbit (only Nanedi 905) | self developed |
| UCL | | sub-areas | self developed |
| USGS | V.1: standard | sub-areas (Nanedi 927 not processed) | semi-automatic approach involving ISIS, SOCET SET and some manual interaction |
| | V.2: refinement of V.1 results by shape-from-shading | Candor sub-area | in addition to V.1 self developed |

Table 2: Overview of test participants, processed areas and used software (for the abbreviations see list of authors and affiliations)[4]

[4] Due to unforeseen difficulties the shape-from-shading results of the Munich Bundeswehr University group are still pending. We strive to include their work in the final analysis of the test results.

The deviation of the individual DTM strips to the MOLA DTM were then automatically analysed and adjusted based on piece-wise trend analysis.

**DLR-Gwinner** (Gwinner et al., 2005): *Image pre-processing* consists of space variant filtering and a pre-rectification of the images using the MOLA DTM (and derived HRSC DTM for finer pyramid levels). Least-squares *image matching* is done pair-wise between the nadir channel and the four additional panchromatic channels (stereo and photometry). The size of the search window mimics an epipolar constraint. Point tuples are subsequently generated and *3D points* are computed by least squares forward intersection. In V.1 elimination of 3D blunders based on the procedure of DLR/Gwinner-ipf (see below) is performed, while in V.2 the original object points derived by least squares forward intersection are used for DTM interpolation. *DTMs are created* by distance weighted raster interpolation from multiple object point sets derived at different matching scales. An integral part of this approach are standardised quality checks (e.g. point density and point accuracy depending on matching scale) which serve e.g. for an appropriate selection of the DTM grid size.

**DLR-Gwinner/ipf** (Attwenger et al., 2005): This method uses the 3D points generated by DLR-Gwinner (see above) as input. Subsequently, a classification is carried out, which eliminates gross errors based on iterative linear prediction. Resulting holes were filled by interpolation. The positively classified data set was then returned to DLR (see DLR-Gwinner V.1). A DTM was also generated by ipf using the commercial DTM package SCOP.

**DLR-Hirschmüller** (Hirschmüller et al., 2005; 2006): *Image pre-processing* consists of a projection to a plane and a conversion of the radiometric resolution from 16 to 8 bits. *Image matching* is done pair-wise between the nadir channel and all of the additional panchromatic channels (stereo and photometric) along epipolar lines. The nadir, the two stereo, and the two photometry channels are used. Matching is driven by minimising a cost function involving mutual information (MI, Hirschmüller, 2005). MI is a measure based on the entropy of the two images and the mutual image entropy. Penalty terms are added to the cost function to support piecewise smoothness of the terrain. To reduce outliers matching is done in both directions (left-> right, followed by right -> left), the results from pair wise matching are fused in a robust manner, and peaks in the mean disparity map are removed. *3D points* for every pixel are then computed by forward intersection. Holes in the *resulting DTM* were filled using inverse distance weighted interpolation from the border of holes. Since the memory requirement of the procedure is relatively high processing was carried out in tiles. Finally a DTM with a reduced grid size was computed by the pilot centre using the DLRDTM software tool. The method had originally been developed for handling sharp depth discontinuities during matching as mainly occurring in terrestrial HRSC data of urban areas. The adaptation to Mars scenes consisted only in parameter tuning.

**Purdue (**Rengarajan et al., 2004): In this approach no *image pre-processing* is done. *Image matching* relies on a set of seed points (provided by the pilot centre). A cross correlation is first applied to refine the seed points and remove blunders. The selected seed points are then triangulated in image space based on a Delaunay triangulation. For each corresponding triangle pair a two-dimensional affine transformation is determined using the neighbouring seed points. A point with distinct feature properties within a triangle is then transformed into the second image and is considered as the candidate for matching. The actual corresponding point is found via cross correlation followed by sub-pixel local maximum determination. This process runs iteratively until a desired point density is reached. Matching is done pair-wise between the nadir channel and the two stereo channels. Cross evaluation between the matching pairs is carried out to remove points with large inconsistence. Point tuples are subsequently generated and *3D points* are computed by the least squares forward intersection. A threshold for the intersection accuracy is applied to eliminate blunders. From these 3D points a DTM was generated by the pilot centre with the software DLRDTM using bilinear interpolation. Finally, a 3×3 box filer was used to smooth the result. Only image 905 was processed.

**UCL** (Day et al., 1992; Kim, 2005): *Image pre-processing* consists of a pre-rectification of the images using the MOLA DTM. *Image matching* is based on automatically generated seed points. For the upper third of Candor these were generated using DLRMATCH, for all other areas seed points were generated by software developed at UCL. Matching was carried out in pairs using the nadir and the two stereo strips. For those parts of image 927 without image information (see above) the nadir and the two photometry channels were used instead. The matching method employed was a variant of the adaptive least squares correlation (ALSC, Grün, 1985), which is based on region-growing (Otto and Chau, 1989). The employed matching criterion is the maximum eigenvalue of the variance-covariance matrix of ALSC, which is minimised. Results of pair wise matching are then merged and *3D points are computed* via least squares forward intersection. A threshold for the intersection accuracy is applied to minimize the number of blunders. Edge artefacts were cropped manually based on a visual inspection of the results. Finally, a DTM was interpolated from the results using DLRDTM.

**USGS** (Kirk et al., 2003; 2006): Processing was done within the USGS digital cartographic system ISIS and the commercial SOCET SET system, Version 5.2 (Miller and Walker, 1993; 1995). Neither system is able to handle varying integration time within one orbit (this occurred for Nanedi, see above), neither can the exterior orientation parameters for the HRSC sensor be introduced as input. Therefore, separate image patches with constant integration time were generated for Nanedi by cutting up the image strips accordingly, and the exterior orientation was computed based on ground control points from MOLA tracks measured manually in the images (whereas for Candor the nadir, the two stereo and the four colour channels were included in the bundle adjustment, only the nadir and the stereo channels were employed to for determining the exterior orientation of the Nanedi images). *Image matching* is done using SOCET SET's Adaptive Terrain Extraction module (ATE). The images were pre-rectified using the MOLA DTM. Matching was done in pairs between the nadir channel and stereo channels. The MOLA DTM was used as initial height values. The employed matching criterion is the cross correlation coefficient. Point pairs are then transformed into 3D points by least squares forward intersection, followed by DTM interpolation and merging of the individual DTMs. In this way two different DTMs with a resolution of 75 m and of 300 m were generated. Areas with blunders were identified in stereo in the 75 m DTMs and replaced by corresponding values of the 300 m DTM. In a second manual check remaining errors were corrected and in a number of flat areas of Candor MOLA values were substituted instead. Image 927 from Nanedi could not be processed in the described way. The reason for this is not understood, but it is probably not related to the missing image information in one of the stereo channels (see above) because the image gaps are filled with null data and affect only the placement of control points. A more likely explanation is that the problem relates to

| Step | DLR-Scholten | DLR-Gwinner | DLR-Gwinner/ipf | DLR-Hirschmüller | Purdue | UCL | USGS |
|---|---|---|---|---|---|---|---|
| **Pre-rectification** | yes, using MOLA DTM | yes, using MOLA and preliminary HRSC DTM | | yes, using a plane | no | yes, using MOLA DTM | yes, using affine transform. |
| **Reduction of radiom. noise** | yes (not for V.2) | yes | | no | no | no | no |
| **Epipolar constraint** | indirectly through form of search space | | | yes | no | no | indir. through form of search space |
| **Matching method** | LSM[1] | | | mutual information | cross correlation | ALSC[2] | cross correlation |
| **No. of used channels** | 5 | | | 5 | 3 | 3 | 3 |
| **Image orientation** | standard HRSC sensor model and values derived from bundle adjustment with MOLA DTM as control information | | | | | | self determined |
| **Constant set of parameters** | yes | no | | yes | not applicable | yes | yes |
| **Human interaction[3]** | no | no | no | no | no | no, except man. cropping of edge artif. | yes |

Table 3: Key aspects of the individual matching algorithms ([1]: LSM - Least squares matching, [2]: ALSC - adaptive least squares correlation with region growing, [3]: other than test runs etc. to define process parameters)

| Test participant | DTM resolution | Remarks on selection of DTM resolution |
|---|---|---|
| DLR-Scholten | 200 m | standard value |
| DLR-Gwinner | 75 m, except image 905 and Nanedi mosaic: 50 m | selection based on test runs for point density and accuracy depending on matching resolution |
| DLR- Gwinner / ipf | 35 m, except Nanedi mosaic: 50 m | selection based on input data density |
| DLR-Hirschmüller | 50 m | grid size equivalent to image resolution delivered: 30 m (Candor) and 15m (Nanedi), computation of DTM by pilot centre according to directions of participant |
| Purdue | 200 m | 3D point cloud delivered, computation of DTM by pilot centre according to directions of participant |
| UCL | 50 m (Candor)<br>25 m (Nanedi) | based on visual inspection of intermediate results |
| USGS | 75 m | DTM resolution > image resolution of nadir channel × 3 |

Table 4: Deliverables of the participants

the greater roll angle of the 927 image compared to the others. For the Candor orbit the results were further refined using shape-from-shading (Kirk et al., 2006).

Key aspects of the individual matching approaches are summarised in Table 3, Table 4 contains an overview of the DTM resolution selected by the participants together with a justification for this selection.

## 5. TEST RESULTS AND EVALUATION

In this section we report on the results obtained by analysing the data received from the participants. We have evaluated the DTMs generated by the participants from a global and a local point of view, looking either at the whole test area or at small but representative enlargements. In both cases quantitative and qualitative assessment has taken place.

In the *quantitative* assessment we compared the HRSC DTM to the MOLA data (for a justification see section 2). The *qualitative* assessment consisted of a visual inspection of shaded relief representations of the derived DTMs, an analysis of profiles along the MOLA tracks and in East/West direction[5], a comparison of height contours derived from the DTMs and the underlying HRSC images, and a detection study of small craters in the DTMs. All but the last point are discussed in this paper (the crater detection study is still ongoing at the time of writing – July 2006). Finally, *operational aspects* were assessed. They are discussed with respect to the needed computational time and resources for generating the DTMs.

In the first step we computed the offset (mean difference) and the standard deviation between the derived HRSC DTMs and the MEGDR (Mission Experiment Gridded Data Records, Neumann et al., 2003) along MOLA tracks running through the test areas. Tracks were used rather than the complete test areasin order to make use of the best possible MOLA accuracy and resolution. A graphical representation of the results is presented in Figure 2. In addition we have generated shaded relief representations and colour-coded difference maps of the

[5] For lack of space detailed results from the profile analysis are not shown in the paper. Nevertheless, the profile analysis has contributed to the overall results.

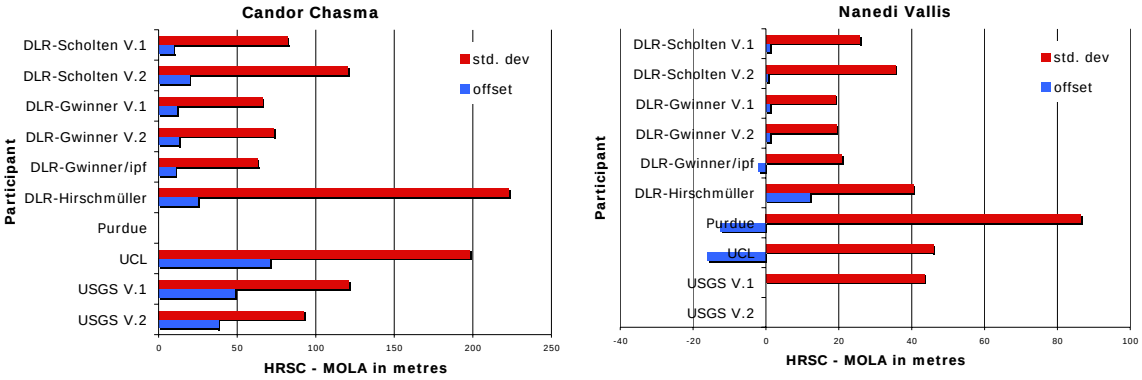


Figure 2: Graphical representation of statistical comparison between HRSC DTMs and the MOLA MEGDR. The given values refer to average values along MOLA tracks 11003 and 11627 (Candor) and 11835, 13977, 16560 and 20315 (Nanedi).

test areas for all submitted DTMs. Sample results of the colour-coded differences are shown in Figure 3.

In general the Candor images were more difficult to process because Candor includes very steep slopes as well as rather feature-less horizontal plateaus. In addition the image quality is not as good as in the Nanedi images. Therefore, the resulting differences are larger. When analysing the results in more detail the following points became apparent:

- Most offsets are rather small. In all cases the exterior orientation parameters were derived by bundle adjustment using MOLA data as control information. In addition, DLR-Scholten, DLR-Gwinner and DLR_Gwinner/ipf adjusted the individual 3D strips to the MEGDR. This explains the relatively small offsets. Some contributions show larger values for a few Candor results. They are probably an indication of problems in the determination of the exterior orientation (USGS) or matching errors which were not eliminated owing to the lack of any a posteriori blunder detection (UCL).
- The standard deviations contain errors of both, the HRSC and the MOLA DTM. A detailed visual comparison of the MOLA tracks and the HRSC images revealed that despite the relatively large MOLA footprint the tracks give a very accurate account of the Mars surface. As a consequence the standard deviation can be interpreted as an error measure of the HRSC DTM (note that this is not true for the complete MEGDR, see also Figure 4 below). In flat areas, and in particular in Nanedi, some participants reached a standard deviation similar to the ground resolution of the nadir image. In areas with steep slopes the accuracy dropped to various pixels. For one matching result (contributions DLR-Gwinner and DLR-Gwinner/ipf for Nanedi), the standard deviation along the *complete* MOLA tracks shows values contained within the ground resolution interval of the nadir image.
- The standard deviations among the participants vary considerably. However, it has to be noticed, that the groups with the lowest standard deviations used the MOLA DTM for pre-rectification and also fitted the individual DTM strips to the MOLA DTM (see Table 3), and that one participant (USGS) used MOLA for filling holes caused by blunder detection in approximately 30 % of the area. While this was valid for creating the best possible results, it does somewhat reduce the significance of the numerical values. The best results were obtained by DLR-Gwinner and DLR-Gwinner/ipf. From these values it is not clear, however, whether the employed blunder removal technique (ipf) actually improves the results.
- The participants who used more than 3 channels have reached better results.
- A comparison between the two versions of DLR-Scholten indicates that radiometric noise reduction (in this case box filtering of the images) and additional box filtering during DTM interpolation has improved the results. This finding is supported by the fact that the shaded relief representations from V.2 look significantly nosier than those of V.1. Comparing the DLR-Gwinner results (space variant filtering and no box filtering) with those from DLR-Scholten further supports the importance of radiometric pre-processing. Note, however, that previous work (Gwinner et al., 2005) shows that noise reduction by box filtering with fixed-size filter windows, in contrast to the space variant technique, often fails to improve point accuracy and density.
- The shape-from-shading technique somewhat improves the results. The quantitative comparison (Figures 2 and 3) indicates, however, that the improvements are related mainly to the local scale (see also Figure 9), while overall (larger scale) differences to MOLA heights tend to persist.
- Commercial software (USGS), software developed for other types of images (DLR-Hirschmüller developed for terrestrial urban HRSC scenes with many height discontinuities) and prototype software (Purdue) yield somewhat less accurate results than approaches specifically developed for planetary images, in particular when dealing with difficult scenes (Candor).
- It was not possible to adequately process images with varying integration time using SOCET SET (USGS, Nanedi). The colour-coded difference map clearly shows long wavelength effects stemming from problems in enforcing consistency between the image segments of constant integration time in the exterior orientation.
- In the shaded relief representation of DLR-Hirschmüller a number of tile borders are visible, in particular for Nanedi.
- While being of a very high nominal resolution the UCL DTMs suffer from a lack of blunder reduction.

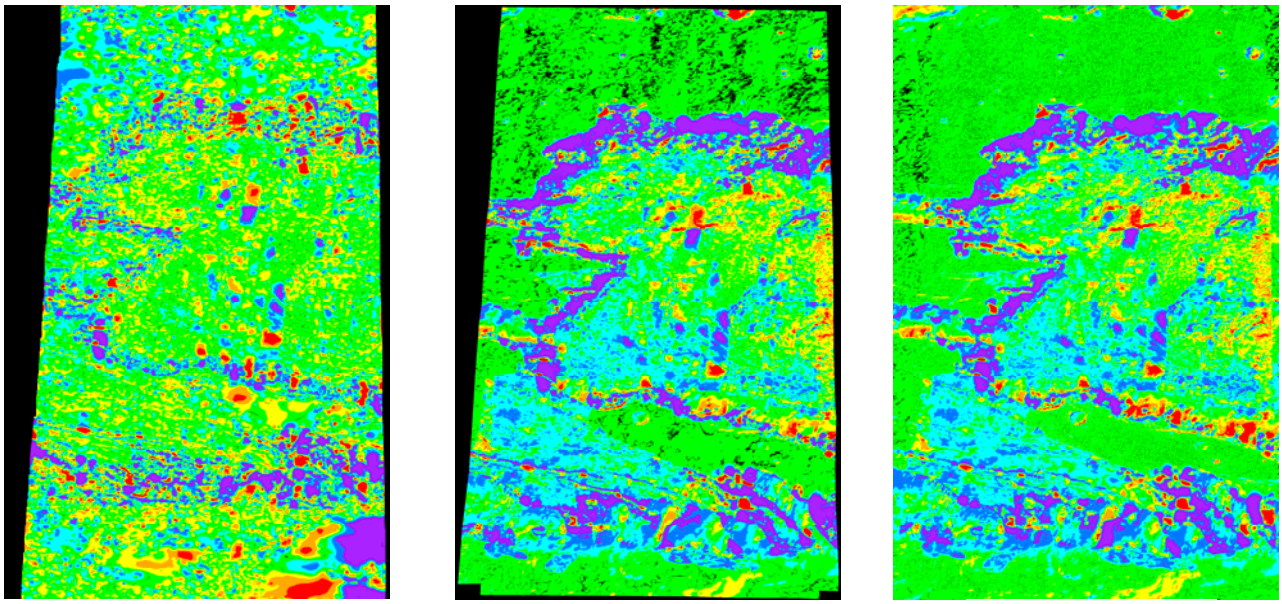


Figure 3: Sample results of colour-coded differences between the HRSC DTM and the MOLA MGDR, sub-area Candor Chasma. From left to right: DLR-Gwinner V.1, USGS V.1, USGS V.2. It can be seen that except for a small area in the lower right the differences are smaller for DLR-Gwinner (see also Figure 2), and that larger differences in the USGS results primarily occur at the steep slopes. The extended green areas in the USGS results stem from the substitution of the matching results by MOLA information. Note that extrema visible in the same location and with the same spatial distribution in all three images are probably MOLA interpolation artefacts rather than errors in the HRSC DTMs. At this scale the two USGS versions show only very few noticeable differences, as is expected given that the explicit intent of the shape-from-shading refinement of USGS V.2 was to improve local details at scales of less than a few km without disturbing long-wavelength components of topography; see Figure 9 for examples of the improvement in fine detail.

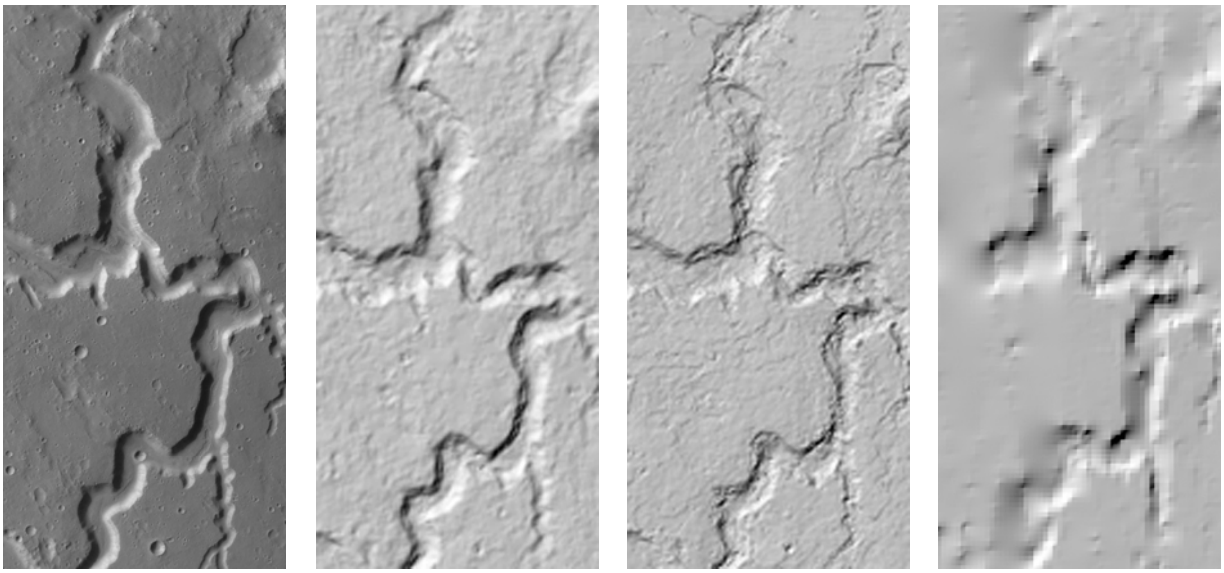

Figure 4: Detail of the Nanedi test area: HRSC nadir image (left), two matching results in shaded relief representation (middle), MOLA MEGDR in shaded relief representation (right). The higher resolution of the matching DTMs is clearly visible. It correlates much better with the image than MEGDR.

Experiments were also conducted with the software, which DLR employs to generate preliminary DTMs using the nominal exterior orientation values as input. These experiments resulted in an offset of up to 100 m in height, this offset being significantly different for the different Nanedi images. Thus, a refinement of the nominal exterior orientation values by bundle adjustment is necessary to consistently tie together different images in a block and to make the results compatible with MOLA (see also Schmidt et al., 2005; Spiegel et al., 2005).

A two-dimensional comparison of a part of the Nanedi test site clearly shows that the MOLA MEGDR can only be considered as a geometric reference along the MOLA tracks. In a two-dimensional comparison the reduced ground resolution of the MEGDR becomes apparent (see Figure 4). Differences between the HRSC DTM and the MEGDR were predominantly found along slopes and undulating terrain. They thus tend to represent the lower resolution of the MEGDR rather than matching errors in the HRSC results. This finding is exemplified in Figure 4, which shows part of the Nanedi nadir image (left) and shaded relief representations of two matching results (middle) in comparison to MEGDR (right). Both test areas are located near the equator. These examples therefore confirm previous reports on improved detail with respect to MEGDR at lower latitudes (Scholten et al. 2005b, Gwinner et al. 2005).

Similar representations are contained in Figure 5, which shows a detail of the Nanedi test site with many craters depicted by thin red circles. Shaded relief representations give a good impression of the quality of delivered DTMs, especially when compared to the HRSC nadir image (lower right). Lower levels of detail can be observed readily for the lowest resolution DTMs when compared to some of the higher resolution DTMs (see Table 4). However, the degree with which additional resolved detail is provided by the contributions with the highest nominal resolution is less obvious. While some approaches are able to generate very consistent results with the impression from the grey value image, others contain considerable noise or artefacts. Again, the difference in ground resolution in comparison to the MOLA DTM is striking. In general the findings from Figure 2 are supported when examining Figure 5 in more detail.

In the next evaluation step height contours were generated from the delivered DTMs. Height contours should represent the general morphology of the terrain. In particular in planetary images with rather constant albedo a comparison with the images gives a very clear indication of the DTM quality. The contours were computed using the approach described in Gehrke et al. (2005) and were superimposed on HRSC orthophotos provided by DLR-Scholten[6]. The contour interval was 250 m for Candor and 100 m for Nanedi. Sample results for areas of $11 \times 17$ km$^2$ are contained in Figures 6, 7 and 8. From these figures differences between the DTMs can be observed, which in many cases correspond rather well to the quantitative results. In Figure 6, for example, the valley is well represented in the height contours of the DLR-Scholten, DLR-Gwinner, DLR-Gwinner/ipf and USGS results, whereas the other contours represent the terrain somewhat less well. In agreement with its 200 m resolution, the contours from DLR-Scholten tend to be less representative at small scale features such as the tributary valleys in the Eastern half of the image. The DLR-Hirschmüller approach seems to generate a nearly vertical wall in the darker part of the valley. In some parts of the contours from Purdue noise and artefacts from the matching result can be found. The lower resolution of the MOLA MEGDR is again clearly visible: the valley can hardly be made out in the contour plot. Note also that some of the smaller craters, which can be seen very well in the images, appear not to be resolved in most DTMs. This is for instance the case for the crater in the centre of Figure 7. Overall, the general trends observed in the other evaluation steps are reinforced by the study of the height contour results.

In Figure 8 also the refinement possible by shape-from-shading can be clearly made out, compare for instance the set of contours in the upper part of the scene. A more detailed view of the potential of shape-from-shading is presented in Figure 9 which shows a significant improvement in terms of visible detail although the quantitative improvement in terms of absolute heights needs further analysis (see Figures 2 and 3). Similar improvements in detail have been demonstrated with other shape-from-shading algorithms (Dorrer et al., 2005). In summary, very detailed DTMs can be generated from the HRSC images. As is visible from Figure 9 and some of the contributions of other participants, at least in some areas it is feasible to use a DTM grid size of three times the resolution of the nadir image.

Finally, the operational aspects of the different algorithms are addressed. In our view, an operational procedure is one which can be used to process large areas (multiple orbits, potentially the whole HRSC data set). Thus, besides accurate and reliable results and a high degree of automation fast generation of the results is a prime indicator of an operational solution. We have chosen to use the computational time necessary to generate the DTMs as reported by the participants as a measure (Table 5). When interpreting the timings one has to keep in mind that different processors and different coding languages were used, in many cases recoding or parallel computing can significantly accelerate the process, and semi-automatic approaches cannot easily be compared with automatic ones in terms of computing time. Also, the DTM resolution chosen by the participants has an often significant influence. However, the choice of an appropriate DTM resolution was a task within the test itself. Therefore, results are not related to the number of DTM posts but to the size of the processed area. In order to have an idea of the number of DTM posts processed, the DLR-Scholten DTM with a grid size of 200 m resulted in approximately 12.6 million points. The times do not necessarily give a true reflection of the computational requirements of the DTM generation procedure, and in particular the matching approach as such. Also, one has to keep in mind that according to current experience the need for additional test runs for many orbits cannot be anticipated prior to starting the work. This is particularly important if highest accuracy and finest detail is a prime requirement. Nevertheless, clear differences can be made out. Not surprisingly, the results with the best operational performance were the DLR contributions offering extensive experience in processing HRSC data.

## 6. CONCLUSIONS

Overall the test was successful and has demonstrated that a number of methods exist, which are able to generate high quality DTMS from HRSC imagery. Nevertheless, noticeable differences in the participants' results were found. Some approaches yield superior results, not surprisingly these are the approaches which were developed with planetary imagery in mind, and those which have been extensively

[6] Strictly speaking each set of contours should have been superimposed on the corresponding orthophoto. However, we had only the DLR-Scholten orthophoto available to us. As a result slight lateral displacements between the contours and the orthophoto may appear, and these should not be interpreted as DTM errors.

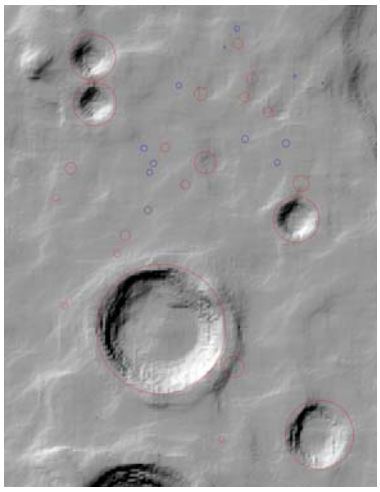

DLR-Scholten V.1

DLR-Gwinner V.1

DLR-Gwinner / ipf

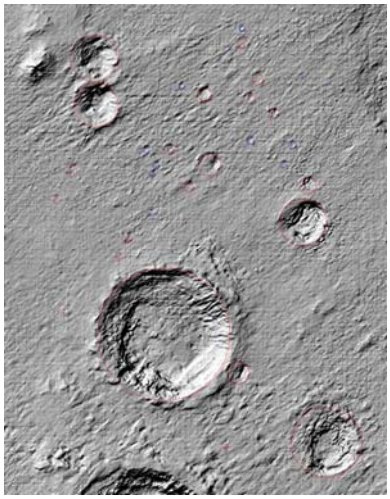

DLR-Hirschmüller

Purdue

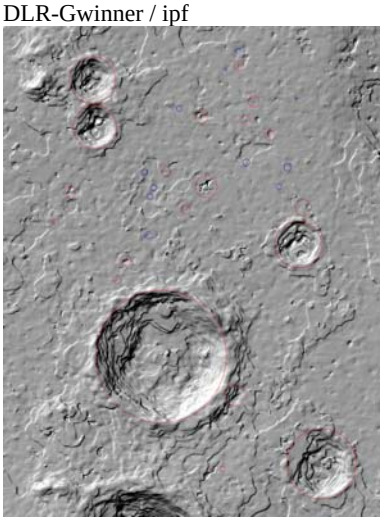

UCL

USGS

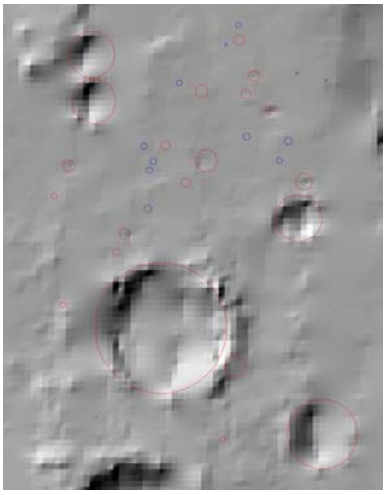

MOLA – MEGDR

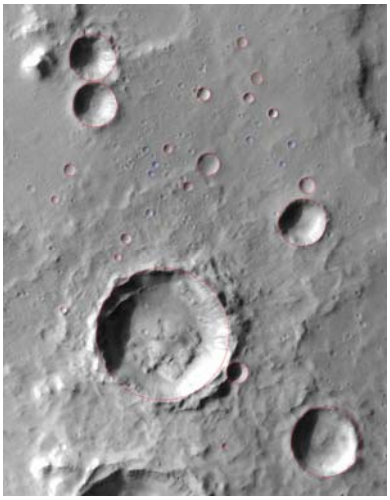

HRSC nadir image

Figure 5: Detail of the Nanedi test site, shaded relief representations of the different DTMs in comparison to HRSC nadir image (lower right)

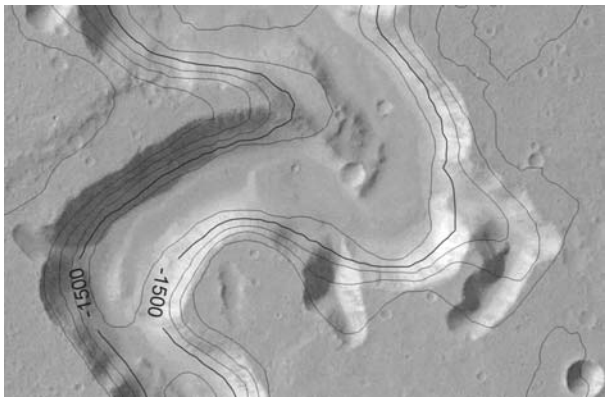


DLR-Scholten, V.1

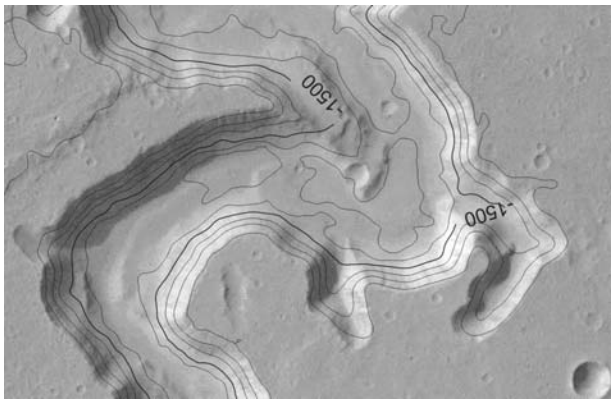


DLR-Gwinner, V.1

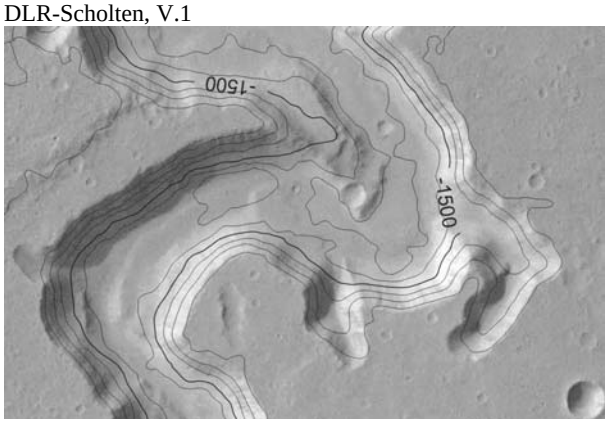


DLR-Gwinner / ipf

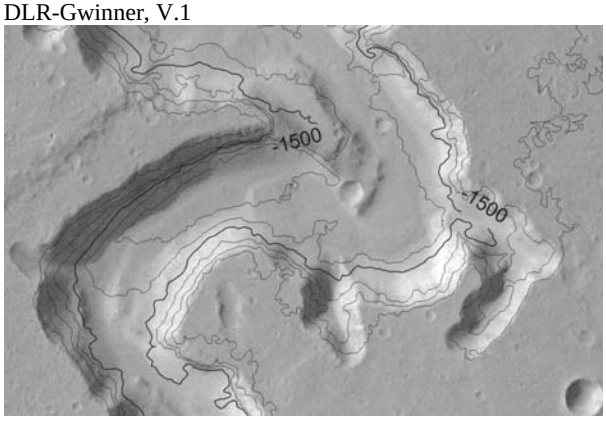


DLR-Hirschmüller

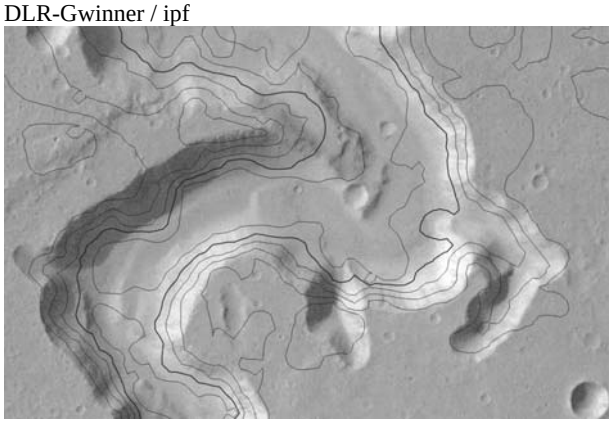

Purdue

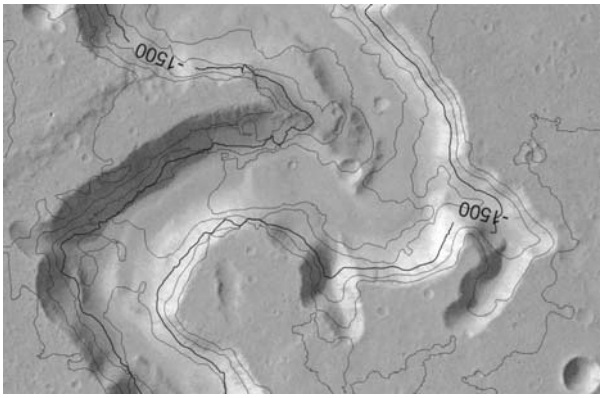


UCL

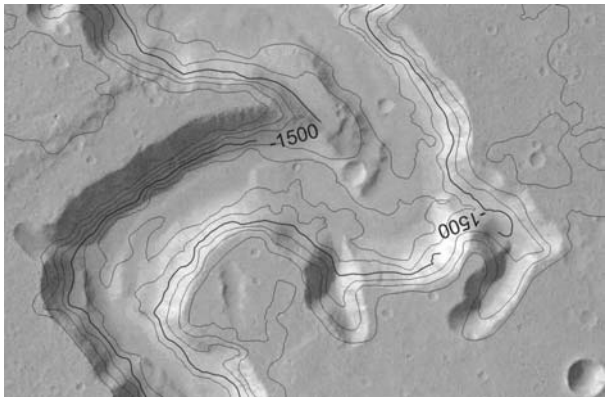


USGS V.1

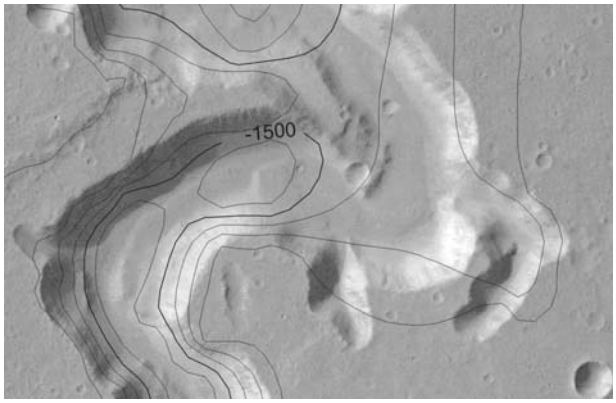


MOLA MEGDR

Figure 6: Part of Nanedi test area (11×17 km$^2$), HRSC orthophoto with superimposed height contours, contour interval 100 m

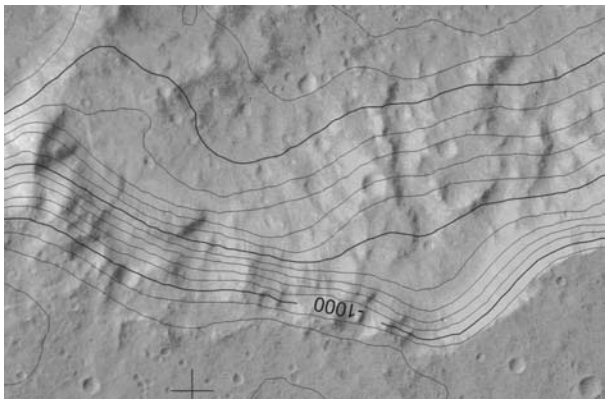


DLR-Scholten, V.1

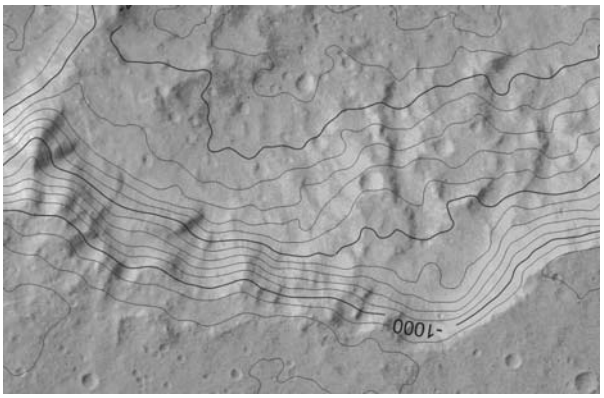


DLR-Gwinner, V.1

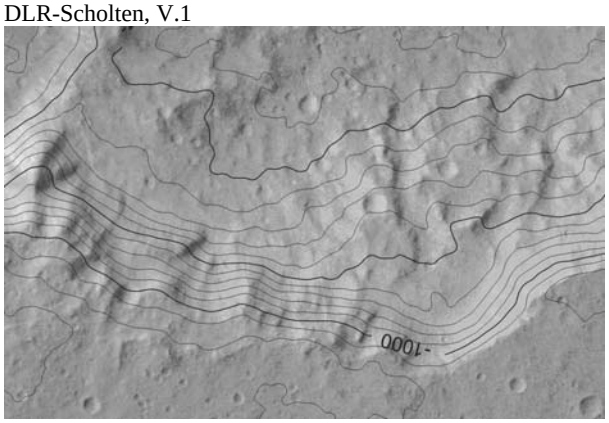


DLR-Gwinner / ipf

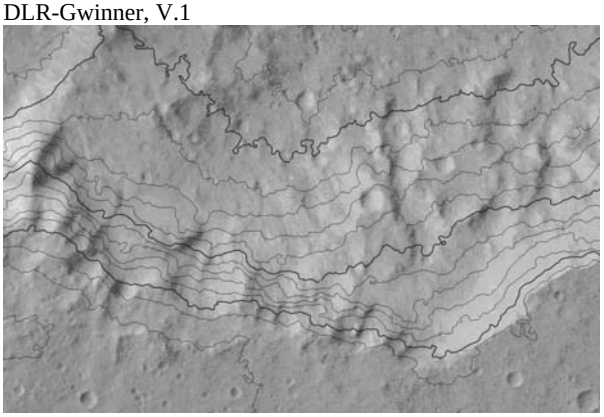

DLR-Hirschmüller

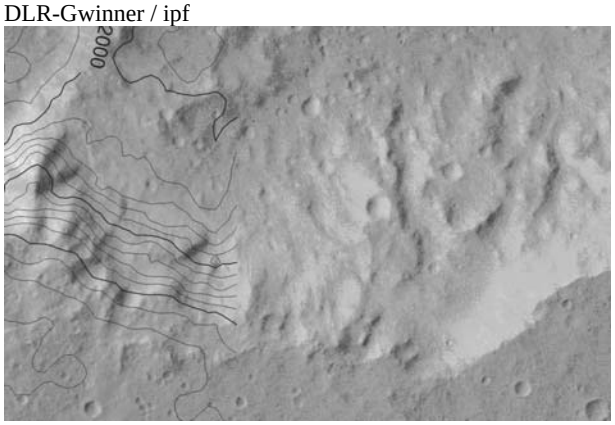


Purdue (no DTM data in right part of image)

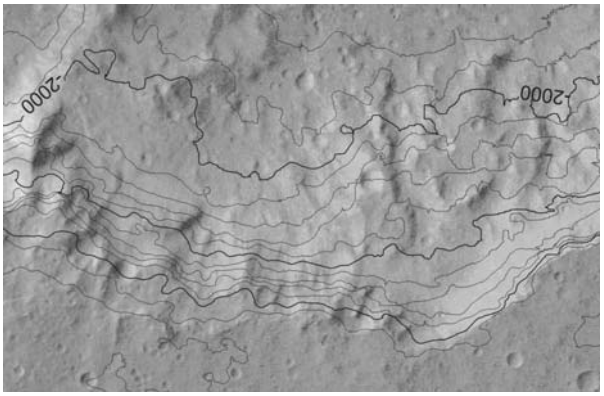


UCL

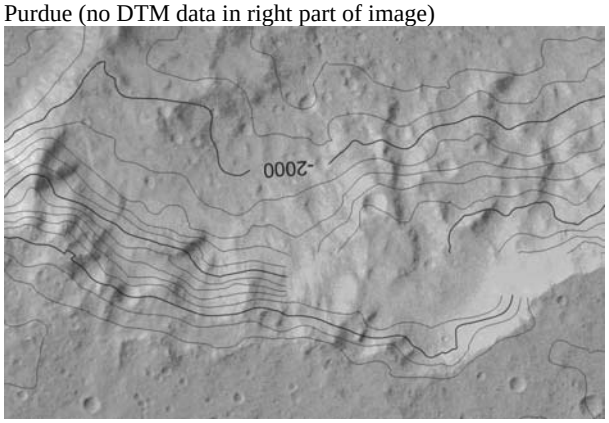


USGS V.1 (data gap in the lower right part)

MOLA MEGDR

Figure 7: Part of Nanedi test area (11×17 km$^2$), HRSC orthophoto with superimposed height contours, contour interval 100 m

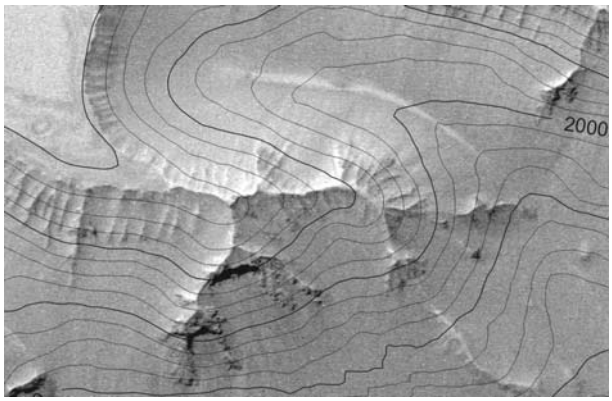


DLR-Scholten, V.1

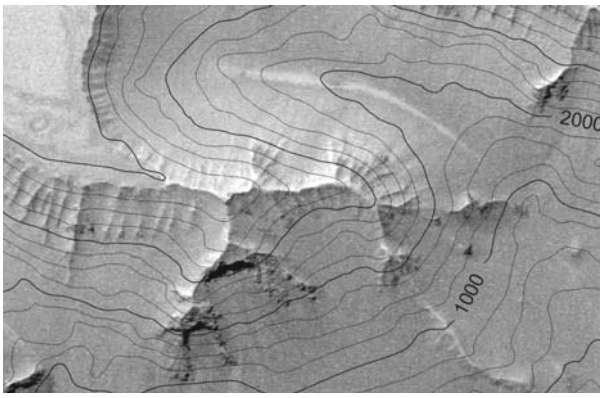


DLR-Gwinner, V.1

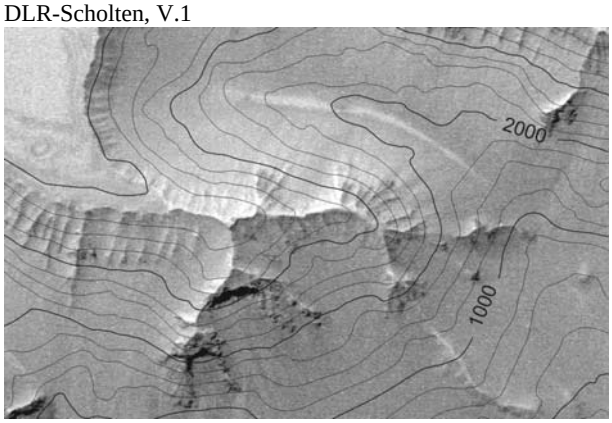


DLR-Gwinner / ipf

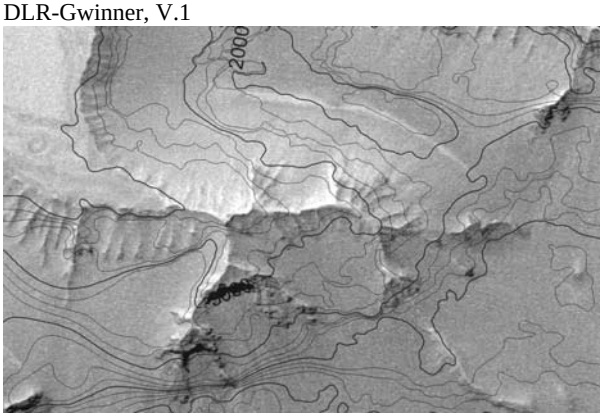


DLR-Hirschmüller

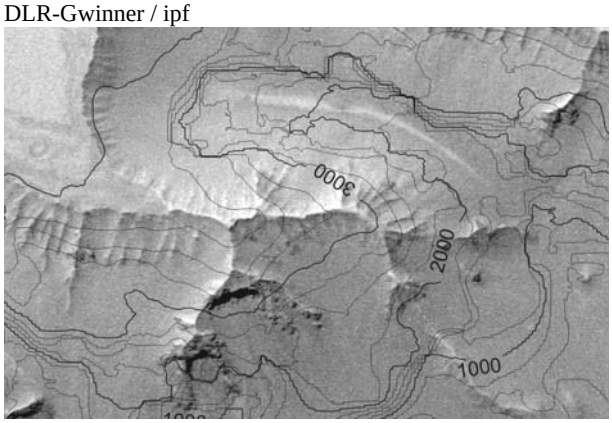


UCL

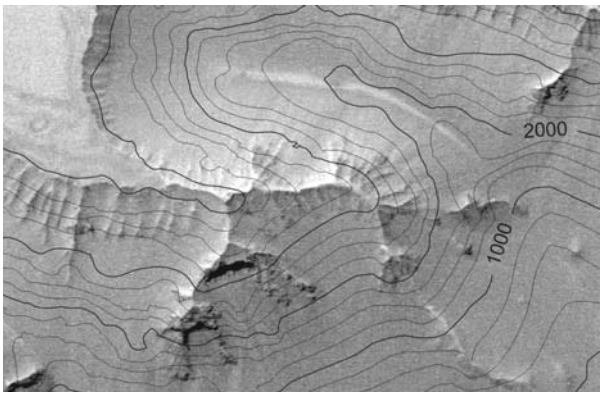


USGS V.1

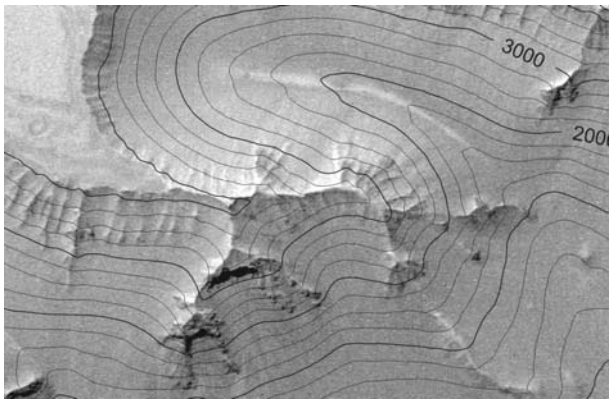


USGS V.2

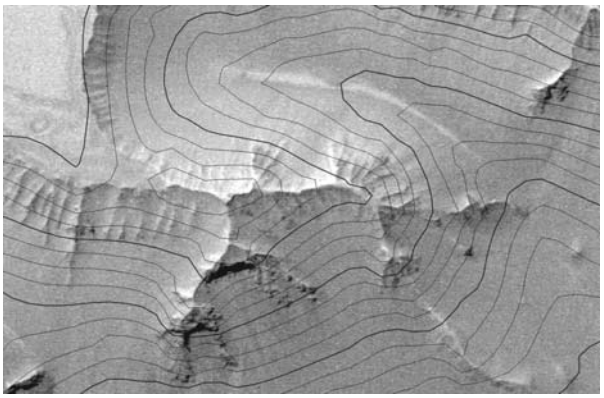

MOLA MEGDR

Figure 8: Part of Candor test area (11×17 km$^2$), HRSC orthophoto with superimposed height contours, contour interval 250 m

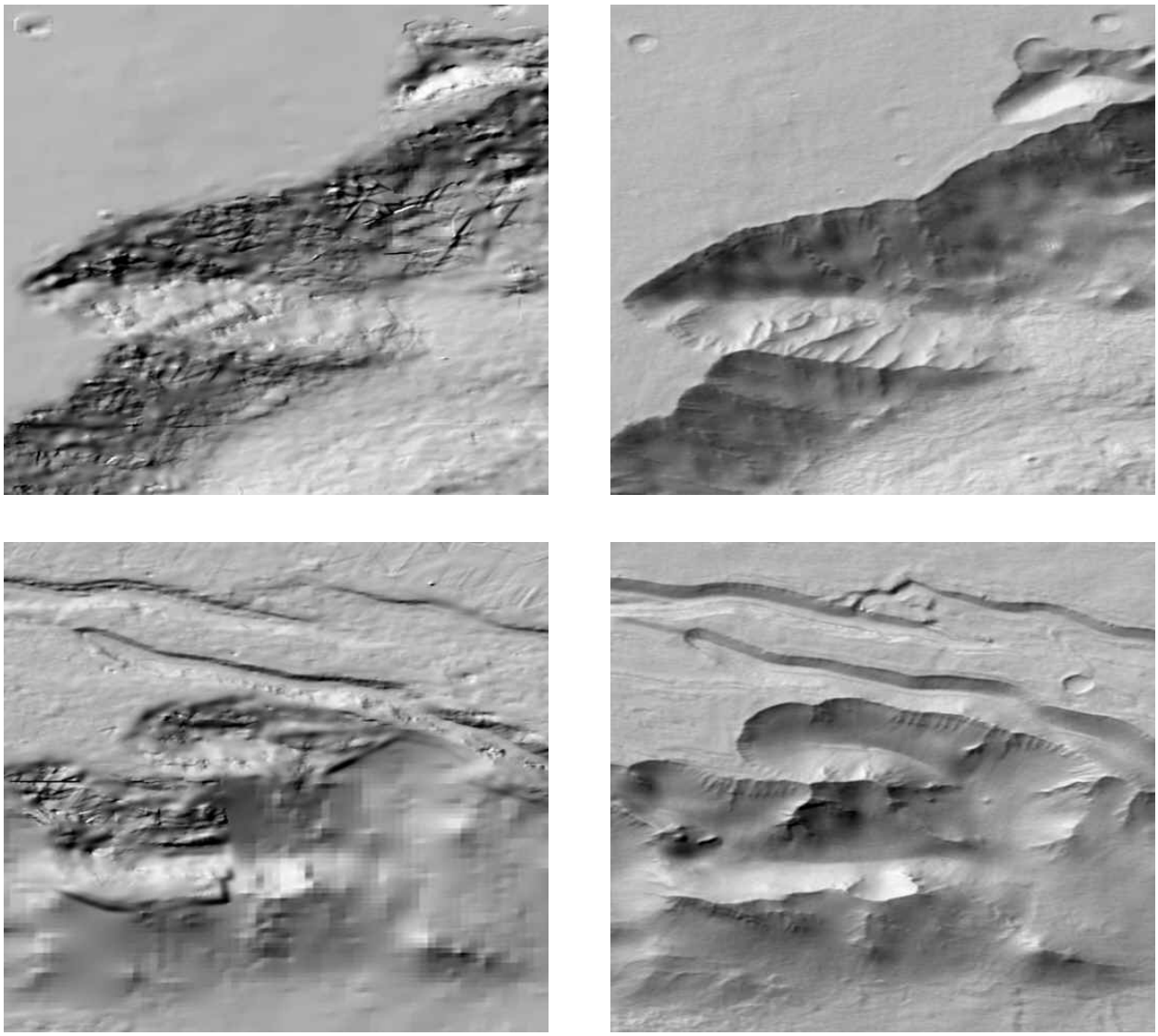

Figure 9: Comparison between the two versions of USGS for two small areas of Candor Chasma in shaded relief representation: before (left) and after (right) refinement by shape-from-shading

applied to planetary and in particular to HRSC image data in the past. While DLR-Scholten and DLR-Hirschmüller turned out to be the most operational methods in terms of processing time (per orbit only few hours are needed), the approaches of DLR-Gwinner and DLR-Gwinner/ipf yielded the best overall results in terms of accuracy and fine detail, still providing operational production times with only a few days processing per orbit. The USGS V.2 solution, which combines a semi-automatic commercial software package with a refinement by shape-from-shading also resulted in remarkable improvement in detail. Furthermore, the test confirms previous findings that the DTMs generated from HRSC data, at least at lower latitudes, are clearly superior to the MOLA MEGDR in terms of resolution and visible fine detail. Very detailed DTMs can be generated from the HRSC images; at least in some areas it appears to be feasible to use a DTM grid size of two to three times the resolution of the nadir image. We will further investigate this aspect in future research using for instance Fourier analysis of DTM profiles and also continue efforts to refine parts of the surface by shape-from-shading.

The geometric accuracy of the derived DTMs varies with terrain characteristics (undulation, texture, etc.). As measured against MOLA tracks a standard deviation of approximately 20 m in height (which corresponds to a ground resolution of one pixel) could be reached for the relatively flat Nanedi test site in the best case. For the more complex Candor Chasma image with a number of steep slopes, less image contrast and more radiometric noise, a standard deviation of two pixels was obtained in the best case. These results correspond to the values which are reached in aerial photogrammetry using image matching and can thus be classified as excellent taking into account the generally low texture of planetary images. While manual editing is known to be able to improve the results particularly with respect to blunder elimination, the test did not focus on evaluating this aspect. Given the sheer amount of data in planetary missions, manual mapping is very costly, and automation is thus the only realistic way to produce results with a reasonable amount of resources. Nevertheless, some manual elimination of blunders may be necessary to achieve highest standards for DTM accuracy, but cost-effectiveness requires that this step be minimized by optimizing the performance of the automated matching.

| Test participant | Performance | | | Hardware | Remarks |
|---|---|---|---|---|---|
| | CPU time [h] | area [$10^3$×km$^2$] | time [min / $10^3$×km$^2$] | | |
| DLR-Scholten | 4 | 500 | 0.48 | 2.8 GHz Xeon | whole orbits<br>noise reduction (V.2) negligible |
| DLR-Gwinner | 277 | 500 | 33.2 | 2.8 GHz Xeon | whole orbits<br>includes CPU time for test runs to tune parameters<br>in addition 36 h manual work required |
| DLR-Gwinner/ipf | 420 | 500 | 40.8 | 2.41 GHz AMD Opteron 250 | whole orbits<br>CPU time includes approximately 80 % of time of DLR-Gwinner |
| DLR-Hirschmüller | 92 | 500 | 11.0 | 2 GHz Opteron | whole orbits<br>time depends largely on matching resolution, can be reduced to under 9 h using 30 m/pixel for all images<br>time can be significantly reduced by parallel processing |
| Purdue | 45 | 90 | 30.0 | 3.1 GHz P4 | whole orbit, Nanedi 905 only |
| UCL | 192 | 113 | 102.0 | 2.4 GHz Xeon | sub-areas<br>elapsed time, hardware shared with other users |
| USGS V.1 | 13.7 + 109 man. | 95 | - | 1.5 GHz Blade 1500 | sub-areas, Nanedi 927 not processed<br>semi-automatic approach, 109 h refers to manual part |
| USGS V.2 | 0.4 | 41 | | 500 MHz G4 laptop | sub-area, Candor 1235 only<br>must be added to timing of V.1 |

Table 5: Operational aspects of different approaches, CPU time for processing both test areas is given (refer to Table 1 for size of individual areas and to Table 4 for employed DTM resolution). UCL time value refers to elapsed time. No values for time/km$^2$ are given for USGS, since this is a semi-automatic approach.

Some inferences can be made for further developments of the matching algorithms: (a) the use of multiple images instead of only the nadir and the two stereo channels often improves the results, (b) the reduction of radiometric noise prior to image matching appears to carry a lot of promise (see also Gwinner et al., 2005), (c) rectifying the images at least to a plane prior to matching is mandatory. More advantageous seems to be a rectification to a DTM such as the MOLA MEGDR or, even better, one generated within the matching process, in particular in areas with steep slopes, (d) detecting and eliminating blunders must be seen as an essential sub-task at every step of the processing chain, (e) general purpose algorithms should be carefully adapted to the peculiarities of the HRSC sensor, e. g. the geometric sensor model, macro pixel formats and varying integration time. We could also show that in order to generate consistent results a photogrammetric bundle adjustment using a sufficient number of tie points is necessary. Control information is provided through the introduction of MOLA data, which also guarantees compatibility with this data set.

While experience in topographic mapping and in particular in planetary mapping can be seen as a significant advantage to obtain good results, in particular when operational aspects are taken into account, exciting developments also take place in the field of computer vision (e. g. Scharstein and Szeliski, 2002). The topographic and planetary mapping community is well advised to closely observe the developments for possible further improvements of their own results.

## 7. REFERENCES


Albertz J., M. Attwenger, J. Barrett, S. Casley, P. Dorninger, E. Dorrer, H. Ebner, S. Gehrke, B. Giese, K. Gwinner, C. Heipke, E. Howington-Kraus, R.L. Kirk, H. Lehmann, H. Mayer, J.-P. Muller, J. Oberst, A. Ostrovskiy, J. Renter, S. Reznik, R. Schmidt, F. Scholten, M. Spiegel, U. Stilla, M . Wählisch., G. Neukum and the HRSC Co-Investigator Team, 2005. HRSC on Mars Express – Photogrammetric and Cartographic Research. *Photogrammetric Engineering & Remote Sensing*, 71(10):1153-1166.

Attwenger, M., G. Neukum und das HRSC Co-Investigator Team, 2005. Klassifikation von HRSC-Objektpunkten zur Generierung hochwertiger Geländemodelle der Marsoberfläche. *Photogrammetrie, Fernerkundung, Geoinformation*, (5):395-402.

Day, T., A.C. Cook, and J.-P. Muller, 1992. Automated digital topographic mapping technique for Mars, *International Archives of Photogrammetry and Remote Sensing*, 29(B4): 801–808.

Dorrer E., H. Mayer, Y. Haases, A. Ostrovskiy, J. Renter, M. Rentsch, S. Reznik, G. Neukum und das HRSC Co-Investigator Team, 2005. Verbesserung räumlicher Daten durch „Shape-from-Shading“. *Photogrammetrie, Fernerkundung, Geoinformation*, (5):403-408.

Gehrke S., G. Neukum und das HRSC Co-Investigator Team, 2005. Das kartographische Softwarepaket Planetary Image Mapper (PIMap). *Photogrammetrie, Fernerkundung, Geoinformation*, (5):417-422.

Grün A., 1985. Adaptive least squares correlation: a powerful image matching technique. South African Journal of Photogrammetry, Remote Sensing and Cartography, 13(3):175-187.

Gwinner, K., F. Scholten, M. Spiegel, R. Schmidt, B. Giese, J. Oberst, R. Jaumann, G. Neukum und das HRSC Co-Investigator Team, 2005. Hochauflösende Digitale Geländemodelle auf der Grundlage von Mars Express HRSC-Daten. *Photogrammetrie, Fernerkundung, Geoinformation*, (5):387-394.

Hirschmüller H., 2005. Accurate and efficient stereo processing by semi-global matching and mutual information, in *Proceedings of the IEEE Conference on Computer Vision and Pattern Recognition*, 20-26 June 2005, San Diego, CA, USA, Volume 2, pp. 807-814.

Hirschmüller, H., F. Scholten and G. Hirzinger, G., 2005. Stereo vision based reconstruction of huge urban areas from

an airborne push broom camera (HRSC), in *Lecture Notes in Computer Science: Pattern Recognition, Proceedings of the 27th DAGM Symposium*, 30.

Hirschmüller, H., H. Mayer, G. Neukum and the HRSC Co-Investigator Team, 2006. Stereo processing of HRSC Mars Express images by semi-global matching. *International Archives of Photogrammetry, Remote Sensing and Spatial Information Sciences*, Vol. XXXVI. Part 4.

Kim J.R., 2005. Landscape object detection and reconstruction by multisensor data fusion, Ph.D. thesis, University College London, 412 p.

Kirk, R. L., E. Howington-Kraus, B. Redding, D. Galuszka, T.M. Hare, B.A. Archinal, L.A. Soderblom, and J.M. Barrett, 2003. High-resolution topomapping of candidate MER landing sites with Mars Orbiter Camera Narrow-Angle images, *Journal of Geophysical Research*, 108(E12), 8088, doi:10.1029/2003JE002131.

Kirk, R.L., E. Howington-Kraus, D. Galuszka, B. Redding and T.M. Hare, 2006. Topomapping of Mars with HRSC Images, ISIS, and a Commercial Stereo Workstation, *International Archives of Photogrammetry, Remote Sensing and Spatial Information Sciences*, Vol. XXXVI. Part 4.

Miller, S.B. and A. S. Walker,1993. Further developments of Leica digital photogrammetric systems by Helava, *ACSM/ASPRS Annual Convention and Exposition Technical Papers*, 3, 256–263.

Miller, S. B. und A. S. Walker, 1995. Die Entwicklung der digitalen photogrammetrischen Systeme von Leica und Helava, *Zeitschrift für Photogrammetrie und Fernerkundung*, 63(1):4–16.

Neukum, G., R. Jaumann and the HRSC Co-Investigator Team, 2004. HRSC: The High Resolution Stereo Camera of Mars Express. *ESA Special Publications* SP-1240.

Neumann, G.A., F.G. Lemoine, D.E. Smith and M.T. Zuber, 2003. The Mars Obiter Laser Altimeter archive: Final precision experiment data record release and status of radiometry, *Lunar Planetary Science* XXXIV, Lunar and Planetary Institute, Houston.

Otto, G.P. and G.P., Chau, T. K. W., 1989. Region-Growing algorithm for matching of terrain images, *Image and Vision Computing, (7)*:83 - 94,.

Rengarajan, R., J.-S. Yoon and J. Shan, 2004. Triangulation based hierarchical image matching for Mars DEM generation using MOC NA stereo images, Annual Convention of the ASPRS, 12 p. (on CD-ROM).

Scharstein D. and R. Szeliski, 2002. A taxometry and evaluation of dense two-frame stereo correspondence algorithms. *International Journal of Computer Vision*, 47(1/2/3):7-42.

Schmidt, R., C. Heipke, R. Brandt, G. Neukum und das HRSC Co-Investigator Team, 2005. Automatische Bestimmung von Verknüpfungspunkten in HRSC-Bildern der Mars Express Mission. *Photogrammetrie, Fernerkundung, Geoinformation*, (5):373-379.

Schmidt R., C. Heipke, G. Neukum and the HRSC Co-Investigator Team, 2006. Improving Tie Point Extraction by Anisotropic Diffusion, *International Archives of Photogrammetry, Remote Sensing and Spatial Information Sciences*, Vol. XXXVI. Part 4.

Scholten, F., K. Gwinner, T. Roatsch, K.-D. Matz, M. Wählisch, B. Giese, J. Oberst, R. Jaumann, G. Neukum and the HRSC Co-Investigator Team, 2005. Mars Express HRSC data processing – Methods and operational Aspects, *Photogrammetric Engineering & Remote Sensing*, 71(10):1143-1152.

Scholten, F., T. Roatsch K. Gwinner, K.-D. Matz, V. Mertens, J. Flohrer, M. Wählisch, B. Giese, R. Pischel, J. Oberst, R. Jaumann, G. Neukum und das HRSC Co-Investigator Team, 2005. Von Rohdaten aus dem Mars Express Orbit zu Digitalen Marsoberflächenmodellen und Orthobildern – Operationelle Verarbeitung von HRSC Daten, *Photogrammetrie, Fernerkundung, Geoinformation*, (5): 365-372.

Smith, D. E., M. T. Zuber, H. V. Frey, J. B. Garvin, J. W. Head, D. O. Muhleman, G. H. Pettengill, R. J. Phillips, S. C. Solomon, H. J. Zwally, W. B. Banerdt, T. C. Duxbury, M. P. Golombek, F. G. Lemoine, G. A. Neumann, D. D. Rowlands, O. Aharonson, P. G. Ford, A. B. Ivanov, C. L. Johnson, P. J. McGovern, J. B. Abshire, R. S. Afzal and X. Sun, 2001. Mars Orbiter Laser Altimeter: Experiment summary after the first year of global mapping of Mars, *J. Geophys. Res., 106(E10*), pp. 23689-23722.

Spiegel, M., U. Stilla, B. Giese, G. Neukum und das HRSC Co-Investigator Team, 2005. Bündelausgleichung von HRSC Bilddaten mit Mars Observer Laser Altimeter-Daten als Passinformation. *Photogrammetrie, Fernerkundung, Geoinformation*, (5):381-386.

Spiegel M., U. Stilla and G. Neukum, 2006. Improving the Exterior Orientation of Mars Express Regarding Different Imaging Cases, *International Archives of Photogrammetry, Remote Sensing and Spatial Information Sciences*, Vol. XXXVI. Part 4.

Zuber, M. T., D. E. Smith, S. C. Solomon, D. O. Muhleman, J. W, Head, J. B. Garvin, J. B. Abshire, J. L. Bufton, 1992. The Mars Observer Laser Altimeter Investigation. *J. Geophys. Res., (97) E5*, pp. 7781–7797.